Developmental Cell
Article

A Rho GTPase Signal Treadmill Backs a Contractile Array

Brian M. Burkel,[1] Helene A. Benink,[1] Emily M. Vaughan,[2] George von Dassow,[4] and William M. Bement[1,2,3,*]
[1]Department of Zoology
[2]Program in Cellular and Molecular Biology
[3]Laboratory of Cell and Molecular Biology
University of Wisconsin-Madison, 1525 Linden Drive, Madison, WI 53706, USA
[4]Oregon Institute of Marine Biology, University of Oregon, 63466 Boat Basin Road, Charleston, OR 97420, USA
*Correspondence: wmbement@wisc.edu
http://dx.doi.org/10.1016/j.devcel.2012.05.025

SUMMARY

Contractile arrays of actin filaments (F-actin) and myosin-2 power diverse biological processes. Contractile array formation is stimulated by the Rho GTPases Rho and Cdc42; after assembly, array movement is thought to result from contraction itself. Contractile array movement and GTPase activity were analyzed during cellular wound repair, in which arrays close in association with zones of Rho and Cdc42 activity. Remarkably, contraction suppression prevents translocation of F-actin and myosin-2 without preventing array or zone closure. Closure is driven by an underlying "signal treadmill" in which the GTPases are preferentially activated at the leading edges and preferentially lost from the trailing edges of their zones. Treadmill organization requires myosin-2-powered contraction and F-actin turnover. Thus, directional gradients in Rho GTPase turnover impart directional information to contractile arrays, and proper functioning of these gradients is dependent on both contraction and F-actin turnover.

INTRODUCTION

Transient contractile arrays of actin filaments (F-actin) and myosin-2 are used by cells and tissues to drive a variety of processes, including cell division, morphogenesis, and wound repair (Bement et al., 2006). Such arrays form at the appropriate place and time, often as a continuous ring, contract to dispatch their biological function, and then disassemble. Contractile array formation is typically controlled by Rho and Cdc42, GTPases that stimulate myosin-2 activation and actin assembly when in their active (GTP-bound) state (Jaffe and Hall, 2005). The Rho GTPases, in turn, are activated by guanine nucleotide exchange factors (GEFs), which stimulate the exchange of GDP for GTP, and inactivated by the GTPase-activating proteins (GAPs), which stimulate the hydrolysis of GTP to GDP (Jaffe and Hall, 2005).

Two ideas have long dominated conceptualization of contractile array formation and function. First, studies of the cytokinetic apparatus (the archetypical transient contractile array) led to the logical idea that contractile arrays direct their own closure by myosin-2-powered shortening (e.g., Schroeder, 1973), an idea subsequently adopted for other kinds of contractile arrays. Second, the Rho family GTPases are thought to function in a fashion wherein GTPase activation by GEFs is separated from GTPase inactivation by GAPs at a considerable distance and time, such that activation initiates formation of a contractile array, and inactivation is later employed to disassemble the array after it has completed contraction (e.g., Minoshima et al., 2003). However, it is now clear that contraction during morphogenesis is subject to far more intricate regulation than originally thought (Martin et al., 2009; Rauzi et al., 2010). Furthermore, contraction-based shortening of contractile arrays cannot easily explain processes such as unilateral cleavage wherein contractile arrays increase in length coincident with ingression (Schroeder, 1990) nor can it explain the closure of the cytokinetic apparatus under conditions where myosin-2 motor activity is suppressed (e.g., Neujahr et al., 1997; Kanada et al., 2005; Reichl et al., 2008; Fang et al., 2010; Ma et al., 2012). In addition, recent studies suggest that continuous flux of Rho through the GTPase cycle is needed throughout the process of cytokinesis (Bement et al., 2006; Miller and Bement, 2009; Yoshida et al., 2009), challenging conventional notions about Rho family GTPase dynamics in contractile array function.

To characterize the relationship between Rho and Cdc42 turnover and contractile array movement, single-cell wound healing of *Xenopus* oocytes was employed. Healing of plasma membrane damage is a conserved feature of eukaryotic cells, and its failure is associated with a variety of diseases (McNeil and Steinhardt, 2003; Sonnemann and Bement, 2011). In *Xenopus* oocytes (Mandato and Bement, 2001), syncytial *Drosophila* embryos (Abreu-Blanco et al., 2011), and embryonic epithelial cells (Clark et al., 2009), plasma membrane damage elicits rapid assembly and closure of a contractile array around the wound site. Formation of this array is controlled by activation of Cdc42 and Rho in discrete, concentric zones around wounds; the zones close over the wound in concert with the closure of the contractile array (Benink and Bement, 2005).

Here, we find that wound-induced contractile arrays can close in the absence of contraction. Analysis of GTPase turnover using a photoactivation approach reveals that the contractile array is underlain by a gradient of Rho and Cdc42 activity that is controlled by both contraction itself and F-actin turnover. The results directly confirm the existence and importance of GTPase flux during contractile array function, explain how contractile arrays can close without being strictly contractile, and reveal

that contraction and F-actin turnover play unexpected roles in regulation of the Rho family GTPases.

RESULTS

Closure without Contraction

The contractile ring forms around wounds and closes inward at a rate of ~5 μm/min as revealed by imaging of fluorescent actin (Figures 1A and 1B). Contractile ring closure is accompanied by extensive myosin-2-powered cortical flow toward the wound, which can be tracked by following translocation of F-actin, myosin-2, and other material to the wound, providing a convenient readout for myosin-2-powered contraction (e.g., Mandato and Bement, 2001; Munro et al., 2004). Brightest point projections—views generated by overlaying the brightest pixels from each time point into a single image—reveal cortical flow as radial streaks converging on the wound (Figure 1A). Cortical flow is also manifest in movies as translocation of material toward the wound (Movie S1 available online). The mean rate of cortical flow in control cells was not significantly different than that of the forward movement of the contractile ring, as determined by kymograph analysis (Figures 1A and 1B), as expected if myosin-2-powered contraction is responsible for directing closure of the contractile ring.

As a direct test of the relationship between contraction and contractile ring closure, cells were microinjected with C3 exotransferase, a specific inhibitor of Rho that prevents wound-induced myosin-2 activation as judged by inhibition of cortical flow and by staining with an antibody specific for the active, phosphorylated form of nonmuscle myosin-2 light chain (Benink and Bement, 2005). Consistent with previous results showing that actin ring formation is Rho independent (Benink and Bement, 2005), C3 failed to prevent formation of the actin ring (Figure 1A). Remarkably, however, C3 also failed to prevent closure of the actin ring, despite the fact that it abrogated cortical flow (Figure 1A; Movie S1). Indeed, quantification showed that whereas C3 microinjection slowed the closure rate of the actin ring by no more than ~50%, it resulted in essentially complete cessation of forward translocation of F-actin (Figure 1B).

To determine whether these results reflected the myosin-2 suppression per se, rather than Rho suppression, F-actin was monitored following wounding of cells microinjected with Y-27632, which inhibits the Rho kinase responsible for myosin-2 activation (Uehata et al., 1997), or blebbistatin, which directly inhibits myosin-2 activity (Straight et al., 2003). The results were not significantly different than those obtained with C3: an ~50% reduction in the rate of closure of the contractile ring, but a near-complete suppression of cortical flow (Figures 1A and 1B; Movie S1). Higher concentrations of these agents, or their combined use, failed to reduce the closure rate by more than 50%, except in cases where the cells were obviously dying (data not shown). Similar results were obtained when myosin-2, rather than F-actin, was monitored: in controls the rate of myosin-2 flow was not significantly different than the rate of ring closure (~5 μm/min), whereas the suppression of myosin-2 activity via blebbistatin treatment resulted in near-complete cessation of flow, but only a 50% reduction of contractile ring closure velocity (Figures 1C and 1D).

To ensure that these results, which were based on 4D image series with a sampling interval of 6 s, were not underreporting physical translocation of F-actin or myosin-2, independent experiments were performed in which single optical planes were imaged at 1 s intervals. Shorter sampling intervals showed robust cortical flow of actin and myosin-2 in controls but failed to reveal significant forward translocation of either of these contractile ring components following myosin-2 suppression, despite the obvious closure of the contractile rings (Figure S1; Movies S2 and S3). In addition, similar results are obtained when a probe that binds F-actin is employed (Figure S1). In summary, when myosin-2-based contractility is suppressed, the contractile ring closes faster than or in the complete absence of the forward translocation of its core components, F-actin and myosin-2.

Although contraction suppression failed to prevent closure of the contractile ring, it nonetheless consistently changed the degree of organization and dynamic morphology of the ring. At the global level, the contractile rings formed after contraction suppression were often misshapen (e.g., Figure 1A, Y sample; Figure S1, Y, C3, and Bleb. samples). Quantification of the ideal (see Experimental Procedures) versus the observed circumferences of actin rings in control, C3, or Y-27632-microinjected cells revealed that in the latter actin rings were significantly less organized than the controls (Figure 1E). In addition, inspection of kymographs and movies revealed that rings closing after contraction suppression often "creep" forward discontinuously, similar to the forward movement of the leading edges of crawling cells (compare control versus experimental kymographs in Figures 1 and S1 and control versus contraction-suppressed samples in Movies S1, S2, and S3).

The Rho and Cdc42 Zones Close in the Absence of Contraction

The simplest explanation of these results is that the Cdc42 and Rho zones that control F-actin and myosin-2 recruitment to the wounds can also close in the absence of contraction and, in doing so, direct inward-biased assembly of F-actin and myosin-2. To test this point, Cdc42 activity was monitored using RFP-wGBD, which specifically labels active Cdc42 (Sokac et al., 2003) in controls or samples subject to contraction suppression as above. In controls, the Cdc42 zone closed at ~5 μm/min (Figures 2A and 2B), the same rate as determined above for contractile ring closure. Suppression of contraction via C3, Y-27632, or blebbistatin microinjection resulted in no more than 50% reduction of the rate of Cdc42 zone closure, remarkably similar to the results obtained for the contractile ring (Figures 2A and 2B). Likewise, the Rho zone, monitored with GFP- or mCherry-rGBD, which specifically label active Rho (Benink and Bement, 2005), closed at ~5 μm/min in controls and half that rate in Y-27632 or blebbistatin-microinjected cells (Figures 2C and 2D). Because the rGBD and wGBD specifically label the active forms of the GTPases, these results also indicate that forward movement of the zones results from preferential activation of Rho and Cdc42 at the leading edge of their respective zones, even when contraction is suppressed. Brightest point projections and movies failed to reveal any consistent pattern of forward movement of active Cdc42 or Rho in either controls or contraction-suppressed cells (Figures 2A and 2C), precluding us from measuring flow rates for the active GTPases. However,

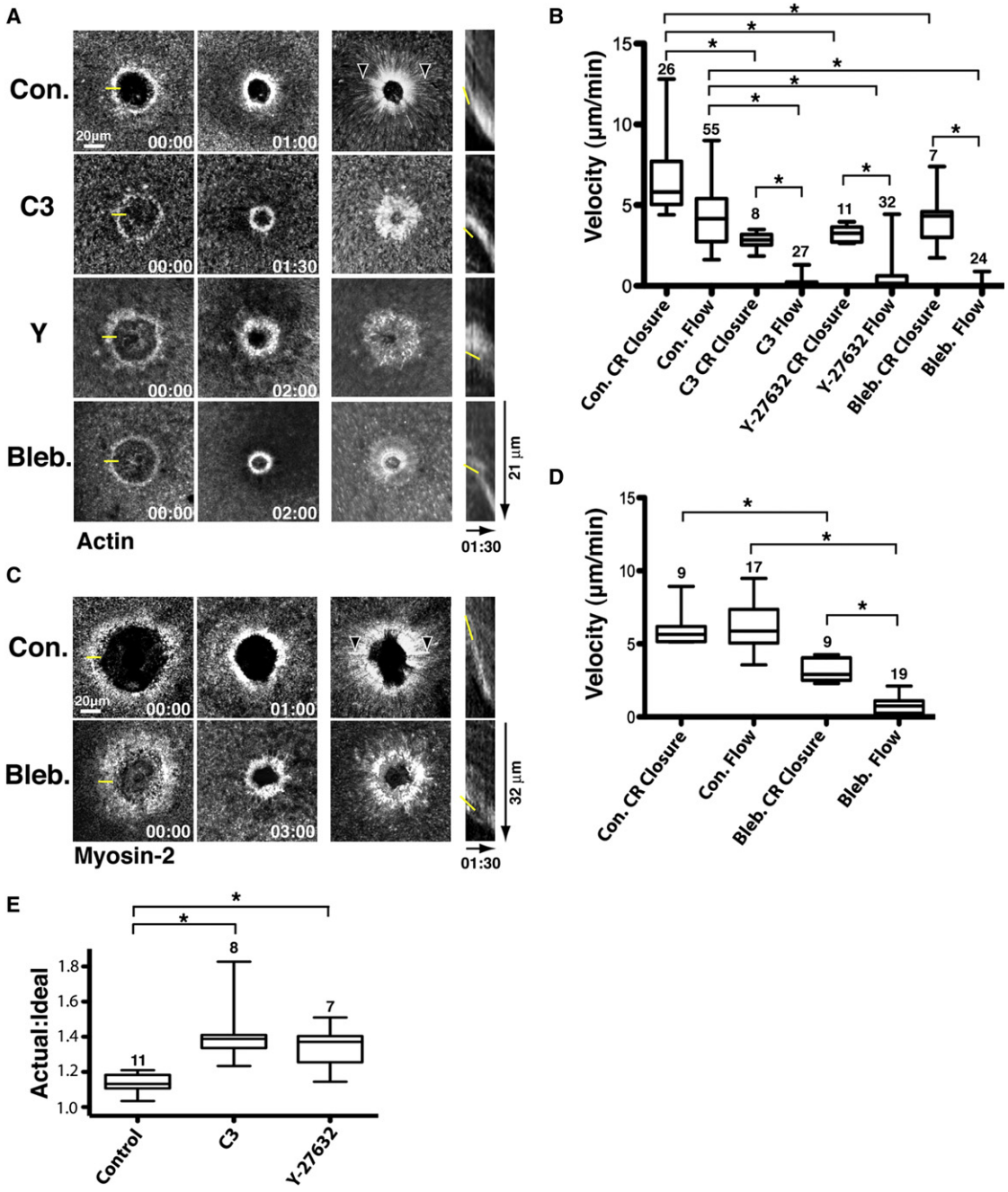

Figure 1. Contractile Ring Closure without Contraction

(A) Actin cortical flow and ring closure. Left: time points, middle: brightest point projections, right: kymographs (from 1 pixel-wide lines) of fluorescent actin following wounding of control (Con.) cells or cells microinjected with C3 exotransferase (C3), Y-27632 (Y), or blebbistatin (Bleb.) to suppress contraction. Yellow line in 00:00 time point indicates where line for kymograph was positioned. Arrowheads in control brightest point projection labels streaks of flowing actin. Yellow line in kymograph identifies position of leading edge. Time is in min:s.

(B) Quantification (using fluorescent actin as a marker) of contractile ring (CR) closure and cortical flow (Flow) in controls and cells microinjected with C3 exotransferase, Y-27632, or blebbistatin to suppress contraction. *$p < 0.05$. Numbers indicate n. Error bars indicate SD.

(C) Myosin cortical flow and ring closure. Layout and labeling are the same as in (A), but fluorescent myosin-2 is used instead of fluorescent actin.

(D) Quantification of myosin flow and ring closure. Layout and labeling are the same as in (B), but fluorescent myosin-2 is used instead of fluorescent actin.

(E) Comparison of the actual to the ideal circumference of contractile rings in control cells and cells microinjected with C3 exotransferase or Y-27632 to suppress contraction. *$p < 0.05$.

See also Figure S1 and Movies S1, S2, and S3.

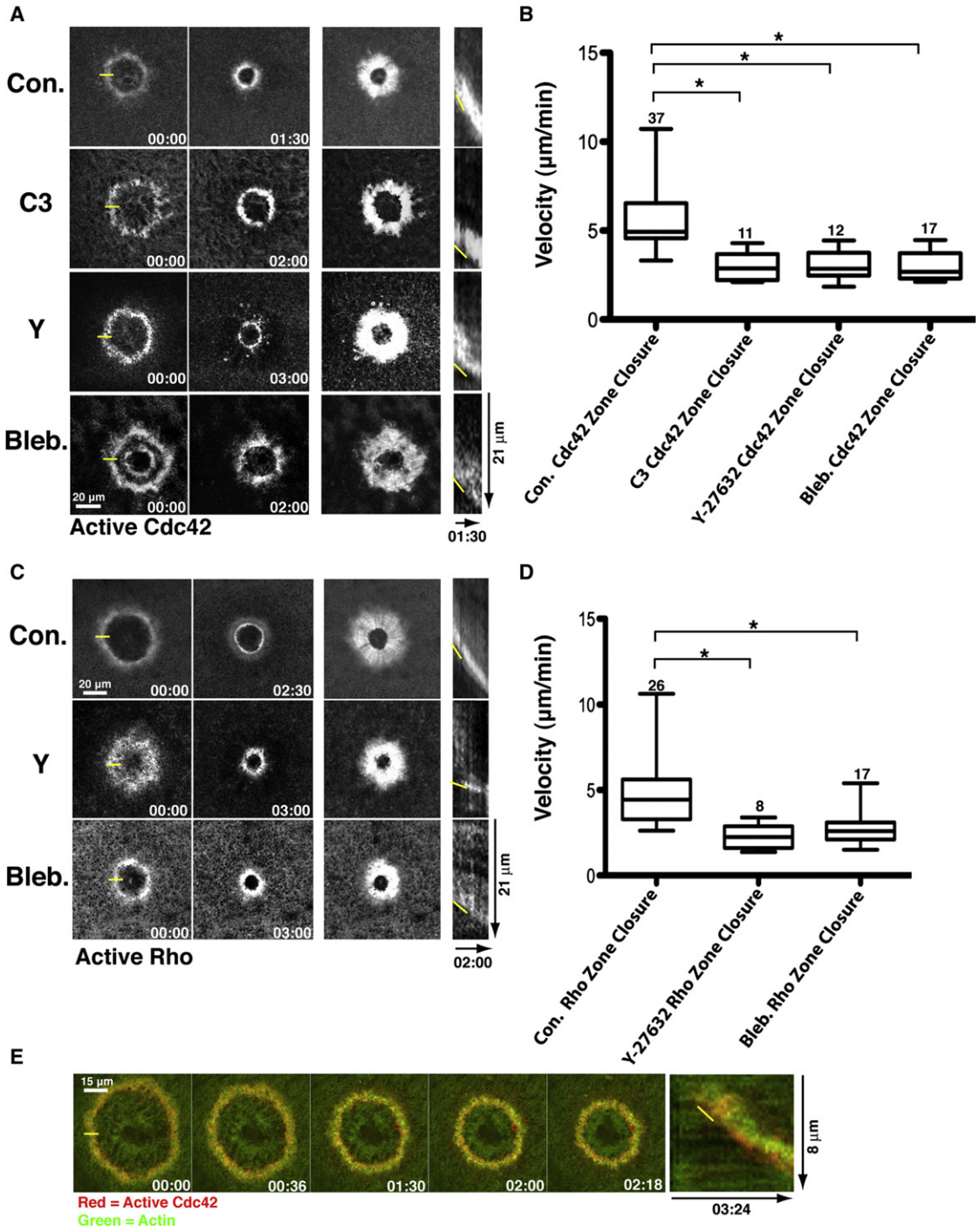

Figure 2. Rho GTPase Zones Close without Contraction

(A) Closure of the Cdc42 zone in controls and contraction-suppressed samples. Layout and labels are the same as in Figure 1A, but fluorescent wGBD is used to detect active Cdc42.

(B) Quantification of Cdc42 zone closure. Layout and labels are the same as in Figure 1B, but fluorescent wGBD is used as a marker.

(C) Closure of the Rho zone in controls and contraction-suppressed samples. Layout and labels are the same as in Figure 1A, but fluorescent rGBD is used to detect active Rho.

(D) Quantification of Rho zone closure. Layout and labels are the same as in Figure 1B, but fluorescent rGBD is used to detect active Rho.

(E) Time course (left) and kymograph (right) showing fluorescent actin (green) and active Cdc42 (red) in C3-injected cell. Yellow line in 00:00 indicates where kymograph line was positioned. Yellow line in kymograph indicates leading edge.

See also Figure S2 and Movie S4.

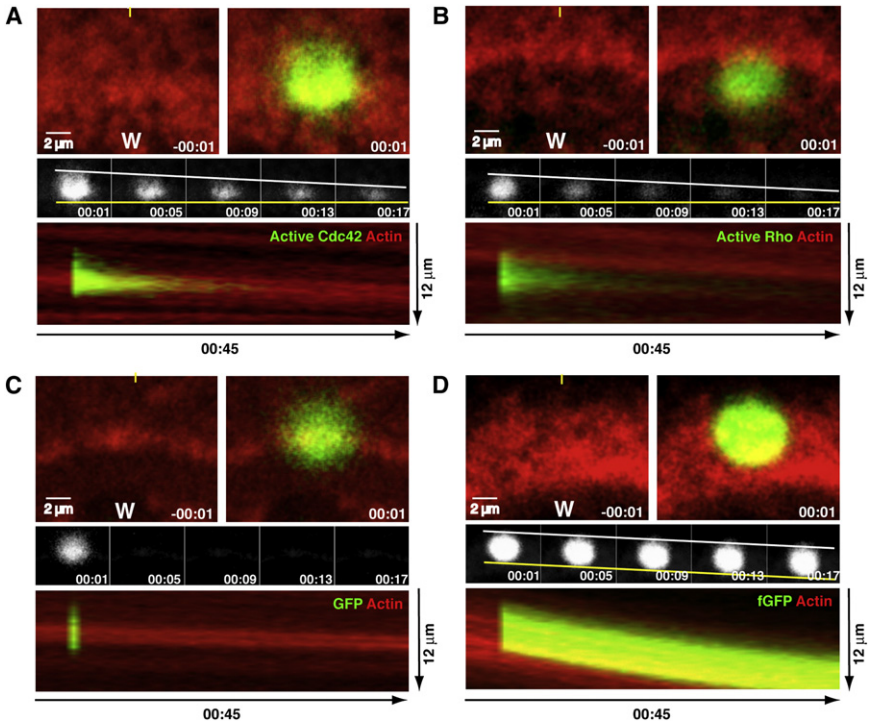

Figure 3. Front-to-Back Bias in Turnover of Active GTPases at Wound Edge

(A) Turnover of active Cdc42 at wound edge assessed with PA-GFP-wGBD (green) and fluorescent actin (red). Top-left panel shows wound (w) edge immediately before photoactivation; top-right panel shows wound edge immediately after photoactivation. Middle panels show active Cdc42 alone from same sample as top, with leading edge of photoactivated region indicated with a yellow line and the trailing edge indicated with a white line. Lowest panel shows kymograph generated from 5-pixel-wide line positioned as indicated by yellow line in top-left panel. The wound is at the bottom of the panel.

(B) Turnover of active Rho at wound edge assessed with PA-GFP-rGBD (green) and fluorescent actin (red). Layout and labels are the same as in (A).

(C) Turnover of probe for soluble proteins at wound edge assessed with PA-GFP (green) and fluorescent actin (red). Layout and labels are the same as in (A).

(D) Turnover of probe for stable PM-associated proteins at wound edge assessed with PA-fGFP (green) and fluorescent actin (red). Layout and labels are the same as in (A).

See also Figure S3 and Movie S5.

as will be shown below, forward movement of active Cdc42 and Rho does not occur until later in the healing process and when it does occur, is slower than the closure of the contractile array.

If, as suggested above, ring closure under conditions of suppressed contraction reflects inward-biased assembly resulting from the closing GTPase zones, it might be predicted that the zones should lead the contractile ring. To test this possibility, double-label experiments were performed in which both actin and active Cdc42 were analyzed after wounding of C3-injected cells. Active Cdc42 did indeed slightly lead actin in such experiments as assessed by both inspection of time points and kymographs (Figure 2E), movies (Movie S4), and line scan intensity measurements (Figure S2).

Photoactivation-Dependent Analysis of Active GTPases

The aforementioned findings are inconsistent with the hypothesis that closure (steering) of the contractile ring or the GTPase zones is driven strictly by myosin-2-powered contraction. An alternative hypothesis is that Cdc42 and Rho undergo spatially biased flux through the GTPase cycle, with preferential activation at the leading edge and preferential loss at the trailing edge of each zone. As noted above, progressive recruitment of the GBD probes to the leading edges of the zones in controls and contraction-suppressed cells is consistent with this hypothesis. However, a comprehensive picture of the GTPase activity cycle requires assessment of their inactivation as well as their activation. Likewise, a means to accurately track the forward movement of the active GTPases is desirable. To accomplish these goals, photoactivatable GFP (PA-GFP; Patterson and Lippincott-Schwartz, 2002) was linked to wGBD (PA-GFP-wGBD) or to rGBD (PA-GFP-rGBD) to monitor both inactivation and potential forward movement of active Cdc42 and Rho, respectively. Because the GBD-based probes have the potential to exchange after binding to the active GTPases, their ability to detect differences in GTPase inactivation was first assessed in unwounded cells by comparing control cells to cells microinjected with GTP-γ-S, a slowly hydrolyzable GTP analog. Although in control cells photoactivated PA-GFPwGBD disappeared entirely within ~2 s, GTP-γ-S microinjection greatly extended the lifetime of the photoactivated PA-GFP-wGBD (Figures S3A and S3B). Similarly, PA-GFPrGBD also disappeared within ~2 s in control cells, whereas GTP-γ-S microinjection extended the PA-GFP-rGBD lifetime (Figures S3C and S3D), indicating that slowing of GTP hydrolysis slows release of the PA-GFP-based probes. To determine whether acceleration of turnover speeds loss of the photoactivated PA-GFP-GBD probes, we first elevated Rho activity using microinjection of mRNA encoding GEF-H1 (a Rho GEF). This manipulation increased the level of active Rho in unwounded oocytes (data not shown) and extended the lifetime of photoactivated PA-GFPrGBD (Figures S3C and S3D). We then compared the turnover of the PA-GFP-rGBD in cells expressing both GEF-H1 and p190 Rho GAP, a Rho-specific GAP. This manipulation accelerated loss of photoactivated PA-GFPrGBD (Figures 3C and 3D), confirming that the PA-GFP-GBD probes faithfully report the inactivation of Rho and Cdc42.

The photoactivatable GTPase activity probes were then used to assess inactivation of Cdc42 and Rho within their respective zones around wounds after the onset of contraction, with fluorescent actin as a marker for contractile ring dynamics (Movie S5). Three striking features of GTPase activity around wounds were revealed by this analysis. First, the overall turnover of Cdc42 and Rho was slowed relative to unwounded cells (compare Figures 3A and 3B, middle panels, to Figures S3A

and S3C, controls; see also below). Second, a distinct spatial bias was evident within the zones, with relatively rapid loss of active Cdc42 and Rho at the trailing (back) edges of the zones and relatively persistent activity at the leading (front) edge of the zones (Figures 3A and 3B, middle and bottom panels). Third, no forward movement of the active GTPases was apparent, despite the fact that the contractile ring (revealed by the actin probe) moved steadily forward in the same time frame (Figures 3A and 3B, middle and bottom panels).

To test the specificity of these results, the behavior of PA-GFP (a reporter for soluble cytoplasmic proteins) and farnesylated PA-GFP (PA-fGFP; a reporter for stable prenylated membrane proteins) was analyzed. PA-GFP dissipated rapidly with no spatial bias relative to the wound (Figure 3C, middle and bottom panels). PA-fGFP turned over very slowly and also showed no spatial bias in turnover (Figure 3D, middle and bottom panels). Furthermore, PA-fGFP, in contrast to the photoactivatable probes for the active GTPases, clearly displayed forward translocation (Figure 3D, middle and bottom panels). Thus, the spatial pattern of PA-GFP-GBD behavior cannot be explained as either a nonspecific consequence of photoactivation in the region of a moving structure nor of, say, bulk endocytosis of membrane proteins.

As an additional test of the specificity of the behavior of the PA-GFP-GBD probes, we monitored Cdc42 activity following overexpression of Abr, a GEF for both Rho and Cdc42 and a GAP for Cdc42 but not Rho (Chuang et al., 1995). This manipulation was previously shown to expand the Rho zone at the expense of the Cdc42 zone (Vaughan et al., 2011). As expected if the loss of PA-GFPwGBD signal reflects GAP-dependent inactivation of Cdc42, Abr overexpression resulted in a sharp reduction of the persistence of active Cdc42 and eliminated the front-to-back bias to active Cdc42 persistence (Figures S3E and S3F). Collectively, these results indicate that the GTPases do indeed undergo spatially biased flux through the GTPase cycle, generating a "signal treadmill," in which Rho and Cdc42 are preferentially activated at or near the leading edge and inactivated or otherwise lost at or near the trailing edge of their respective zones.

Time-Dependent Changes in the Behavior of Active GTPases

To assess temporal features of the signal treadmill, cells were subjected to repeated photoactivation of PA-GFP-wGBD or PA-GFP-rGBD at different times after wounding around the perimeter of the wounds, using fluorescent actin as a reference. This analysis revealed a consistent pattern for both Cdc42 and Rho: shortly after wounding (<30 s), the photoactivated probes were rapidly and uniformly lost from the photoactivated region (Figures 4A and 4B), as they would be in unwounded cells. Next (~30–60 s), the photoactivated region displayed slower loss but with no apparent front-to-back difference (Figures 4A and 4B). At later time points (>60 s), the slower loss was still evident but was accompanied by a front-to-back bias, such that distinct "persistence peaks" of Cdc42 and Rho activity positioned near the leading edge of the zones were evident in kymographs (Figures 4A and 4B).

To assess the relationship between the changes described above and the onset of cortical flow, which commences ~45–80 s postwounding, the half-lives of whole photoactivated regions were first compared. This analysis revealed that the overall half-lives for photoactivated PA-GFP-wGBD and PA-GFP-rGBD within wounds both before and after the onset of contraction were significantly longer relative to either off-wound regions or relative to the PA-GFP probe in either wounded or unwounded cells (Figure 4C). Next, the half-lives of either the front (leading edge) or the back (trailing edge) of photoactivated PA-GFP-wGBD and PA-GFP-rGBD were compared within individual photoactivated regions generated either before or after the onset of cortical flow. This analysis revealed a significant increase in the front-to-back persistence ratio of active Rho and Cdc42 following the onset of cortical flow (Figure 4D). Conversely, quantification of cortical velocity in samples with a front-to-back persistence ratio of less than or equal to one versus those in which the ratio was greater than two revealed that the velocity of the latter was significantly larger than that of the former (Figure 4E). In other words, faster flow was associated with a greater front-to-back difference in the persistence of the active GTPases, and vice versa.

Although forward movement of the active GTPases was rare (Figures 3, 4A, and 4B), it was nonetheless occasionally observed at relatively late times after wounding (>120 s). Examples of this are shown in Figure 4F. This movement, which confirms the ability of the PA-GFP-GBD probes to detect forward translocation of the active GTPases, had two features. First, it was intermittent, with forward movement of active Cdc42 or Rho after a photactivation event in one region being immediately followed by no forward movement in the next photoactivation event of an adjacent region (data not shown). Second, it was significantly slower than the rate of forward movement of contractile ring closure, as judged by comparison of forward translocating active GTPases to actin in the same samples (Figure 4G).

Differentiated Turnover Rates within the Zones

The forgoing results suggested that, following the onset of flow, a turnover gradient develops within the zones such that active GTPases persist considerably longer at the leading than the trailing edges. In principle such a pattern could reflect preferential activation at the leading edge, preferential inactivation at the trailing edge, or some combination of the two. Detecting such patterns by measurement of a single half-life is potentially misleading because some fraction of the photoactivated signal must correspond to free probe. Indeed, inspection of intensity traces over time shows that the intensity profile is poorly fit by a single first-order decay term (Figure S4). We therefore first measured the "half-life" for PA-GFP-rGBD in unwounded cells, i.e., the dissipation rate of free probe in a photoactivated patch (effective half-time of 0.55 s, 101 events). We then fit intensity-over-time data from wounded cells microinjected with AX-568 actin and either PA-GFP-wGBD or PA-GFP-rGBD using a weighted sum of two exponentials—a fast and slow decay rate, with the fast component constrained to the measured turnover rate for free probe (Figure S4). We tested the fidelity of the fitting approach by running the same analysis on cells overexpressing Abr, to accelerate Cdc42 inactivation around wounds (Figure S4). Abr overexpression resulted in an ~2-fold increase in the inferred turnover rate of active Cdc42 around wounds, and an ~3-fold decrease in the putative bound fraction

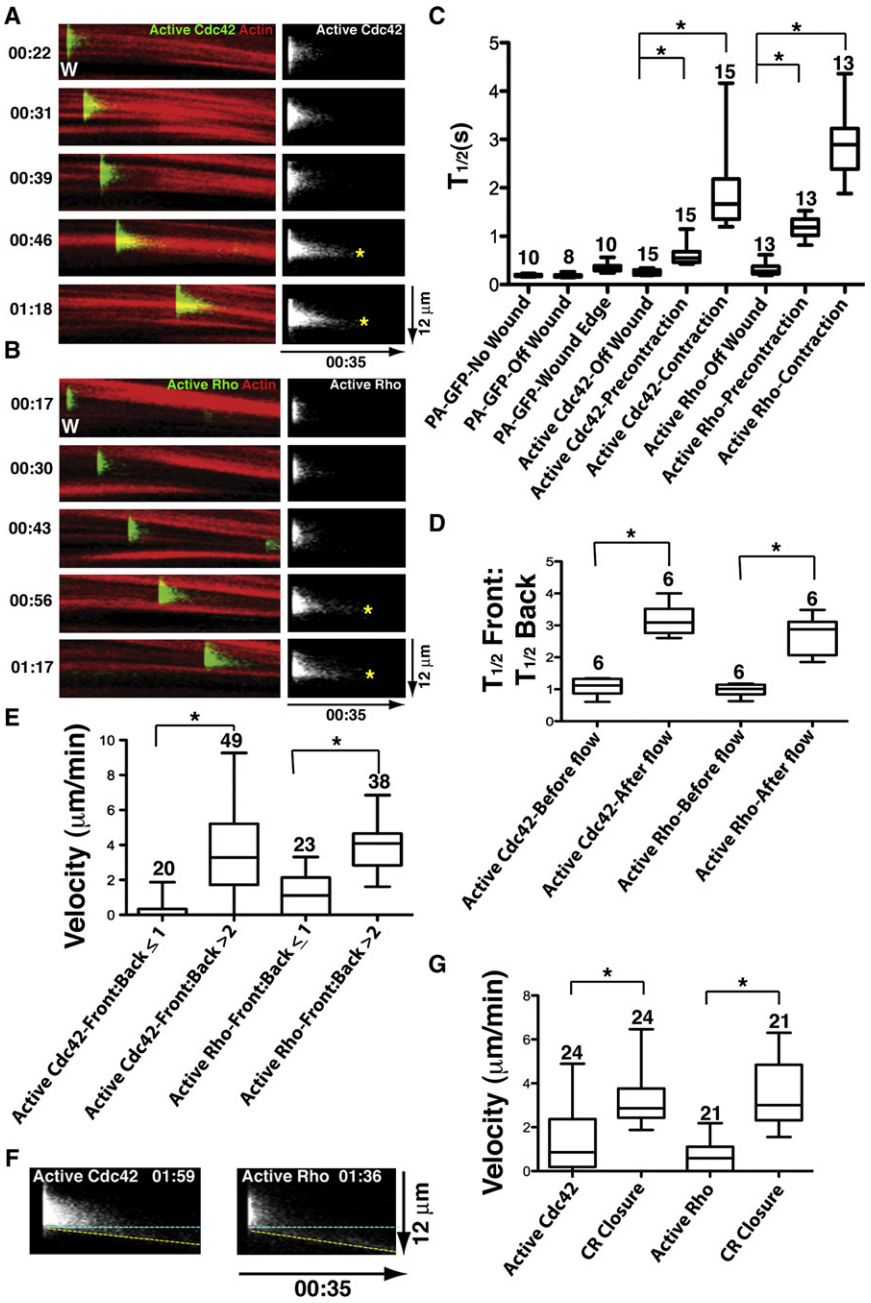

Figure 4. Time-Dependent Changes in the Behavior of Active Rho GTPases

(A) Left panels show kymographs (made as in Figure 3) of turnover of active Cdc42 at wound edge assessed with PA-GFP-wGBD (green) and fluorescent actin (red) at increasing times after wounding (time in min:s indicated on left; each panel from same wound). Right panels show active Cdc42 alone; asterisks indicate persistence peaks.

(B) Turnover of active Rho at wound edge assessed with PA-GFP-rGBD (green) and fluorescent actin. Same layout and labeling as in (A) are shown.

(C) Quantification of total (i.e., entire photoactivated regions) half-life of soluble proteins (PA-GFP), active Cdc42, or active Rho. PA-GFP was assessed in unwounded cells (No Wound), in wounded cells but at >20 μm away from the wound (Off Wound), or at the wound edge after the onset of contraction (Wound Edge). Active Cdc42 and Rho were assessed in wounded cells at >20 μm away from the wound (Off Wound), at the wound (i.e., within their zones) before the onset of contraction (Precontraction), or at the wound after the onset of contraction (Contraction). *$p < 0.05$; numbers indicate n. Error bars indicate SD.

(D) Comparison of the front:back total half-life ratio for active Cdc42 and Rho before (Before flow) and after (After flow) the onset of contraction. *$p < 0.05$.

(E) Comparison of the contractile ring closure velocity when the front-to-back half-life ratio is less than one or greater than two for either active Cdc42 or active Rho. *$p < 0.05$.

(F) Kymographs (made as in Figure 3) showing examples of active Cdc42 and active Rho undergoing forward translocation. Dotted yellow line shows the leading edge of the photoactivated probe; blue dotted line shows expected position of photoactivated probe if it remains stationary.

(G) Comparison of velocity of forward movement of forward translocating active Cdc42 and active Rho versus velocity of contractile ring closure in the same sample. *$p < 0.05$.

(Figure S4), indicating that the fitting approach used does indeed allow detection of GTPase inactivation.

To assess the spatial pattern of GTPase turnover rates within the zones, for each photoactivation event we resliced the image stack in the direction of flow, radially averaged a 4 μm slab containing the center of the patch to create a relatively noise-free kymograph, then fit intensity-over-time data from successive 0.6 μm strips across the GTPase activity zone. Figures 5A and 5B illustrate three representatives for Cdc42 and Rho. We found no consistent spatial pattern for the slow (bound) component of Cdc42 turnover, although the inferred amount of free probe was least in the region that overlapped best with the actin ring. In contrast, we consistently found that the slow component of Rho turnover was slowest at the leading edge. In some cases a smooth gradient was apparent (Figure 5B, top panel); others showed a step-like gradient (Figure 5B, middle and bottom panels). In addition, the inferred fraction of probe bound was lowest in portion of the Rho zone that overlapped the actin ring.

Using the same fitting method, we assessed the change in turnover rate over time for both Cdc42 (in the center of the zone) and Rho (leading versus trailing portions of the zone). This analysis showed that the slow component of PA-GFPwGBD turnover remained nearly constant during wound closure (Figure 5C); this contrasts with the results in Figure 4C, in which free and bound probes are conflated. The increase in the persistence of a patch of photoactivated wGBD probe is therefore due to a steady increase in the bound fraction (data not shown) and,

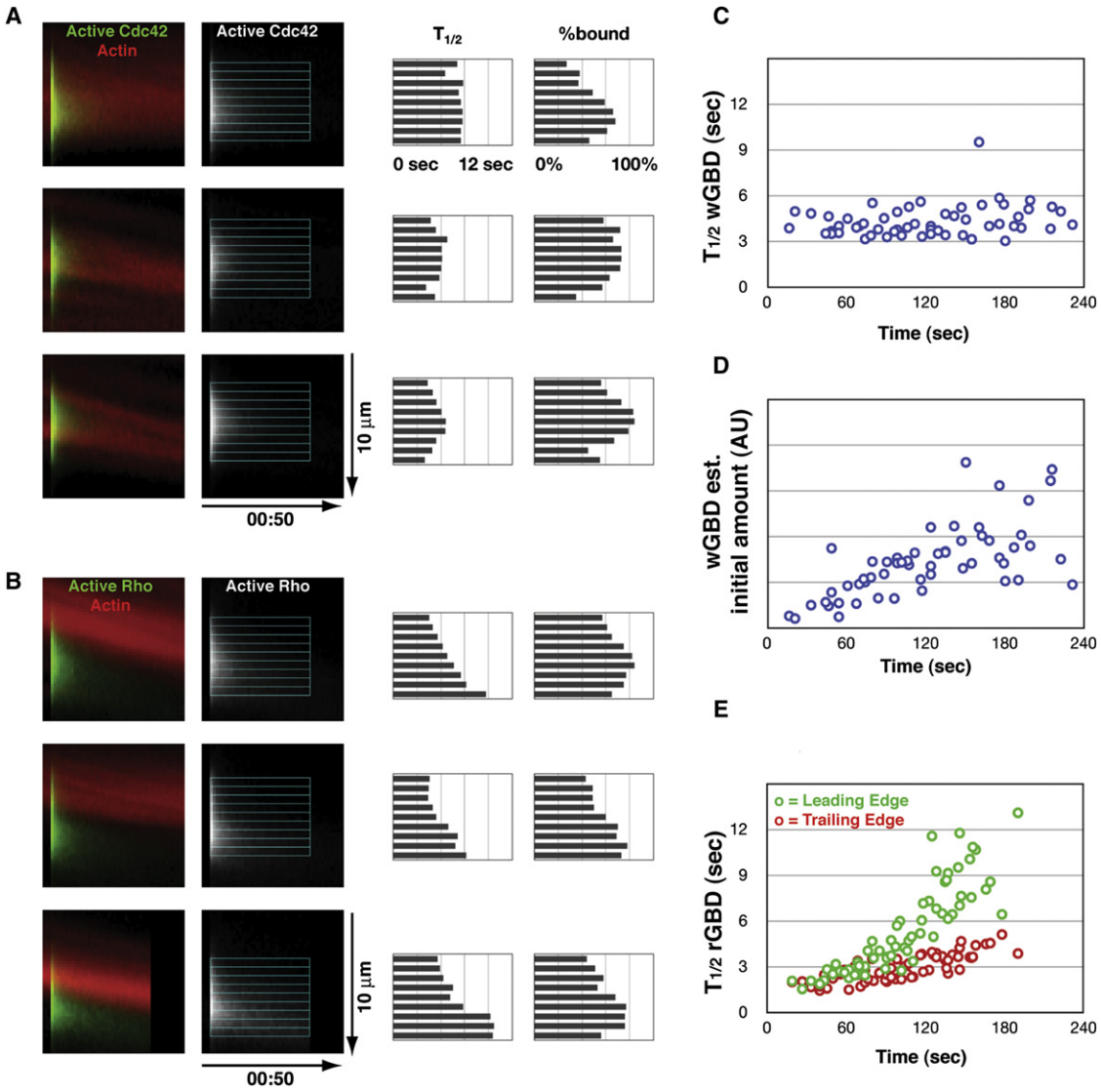

Figure 5. Spatial Differentiation of GTPase Flux

(A) Three examples of a patch of photoactivated PA-GFP-wGBD, represented as kymographs of a 4 μm slab containing the center of the patch. Left panels demonstrate color overlay of PA-GFP-wGBD (green) with fluorescent actin (red), middle panels illustrate PA-GFP-wGBD alone with overlay to show measured 0.6 μm strips, and right panels are bar charts showing half-lives and percentage of probe bound inferred as shown in Figure S4.

(B) Same layout and labels as in (A), but with PA-GFP-rGBD.

(C) Scatterplot of inferred half-time for slow component of wGBD (Cdc42) turnover, versus time since wounding.

(D) Scatterplot of inferred initial amount of wGBD probe bound (arbitrary units: bound fraction times intensity) versus time since wounding, with the same set of measurements as in (C); 60 measurements are shown. AU, arbitrary units; est., estimated.

(E) Scatterplot of inferred half-time for slow component of rGBD (Rho) turnover in leading (green) versus trailing (red) portions of the Rho zone, versus time since wounding. Leading and trailing data points are paired; 64 measurements are shown.

See also Figure S4.

thus, the inferred total amount of bound probe in the initial patch (Figure 5D). PA-GFP-rGBD fits inferred a similar progressive increase in the fraction of bound probe over time (data not shown), but in addition the measured half-lives for the slow component of Rho turnover in leading versus trailing portions of the zone exhibited both a clear increase over the duration of wound closure, as well as an obvious divergence between leading and trailing rates (Figure 5E). In the first minute after wounding, there was no difference between leading and trailing (2.50 versus 2.30 s; 16 events; $p = 0.22$). In the second minute a significant difference had emerged (3.88 versus 2.61 s; 37 events; $p < 10^{-8}$); in the third minute the difference was >2-fold (7.62 versus 3.66 s; 37 events; $p < 10^{-12}$). In other words, these measurements confirm the visual impression that the Rho zone is shaped by a spatial gradient of turnover rate; in contrast, despite a similar visual appearance in kymographs, the spatial patterning of Cdc42 flux must be accomplished at the activation step. This latter conclusion, however, must be qualified: if Cdc42

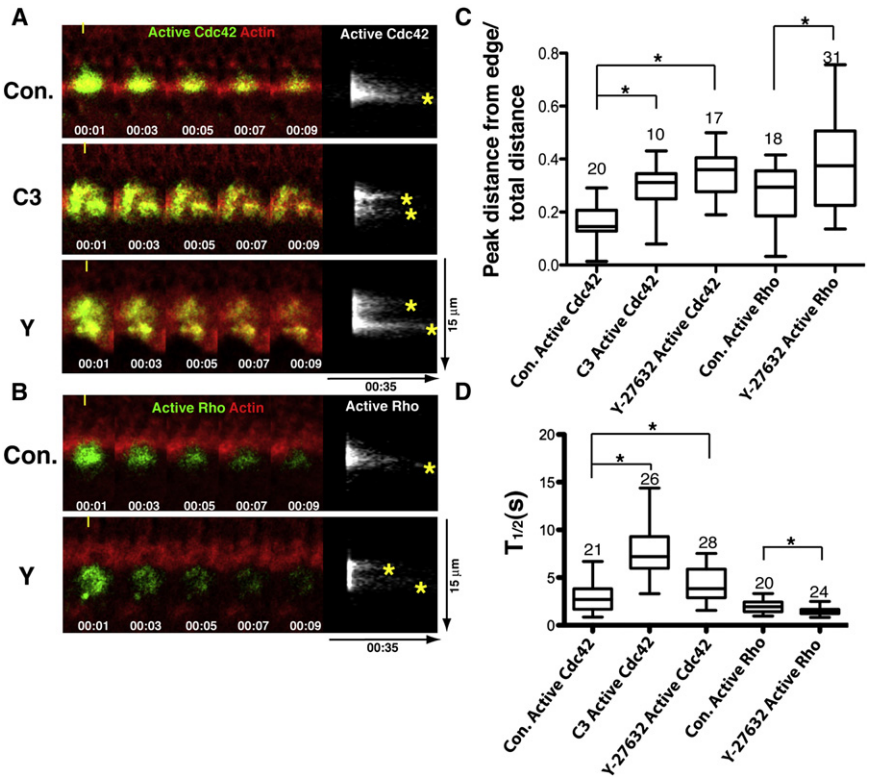

Figure 6. Contractility Is Required for Proper Signal Treadmill Organization

(A) Left panels show kymographs (made as in Figure 3) of turnover of active Cdc42 at wound edge assessed with PA-GFP-wGBD (green) and fluorescent actin (red) in controls (Con.) or cells microinjected with C3 exotransferase (C3) or Y-27632 (Y) to suppress contraction. (Time in min:s indicated on left; each panel from same wound.) Right panels show active Cdc42 alone; asterisks indicate persistence peaks.

(B) Turnover of active Rho at wound edge assessed with PA-GFP-rGBD (green) and fluorescent actin (red) in controls or cells microinjected with Y-27632 to suppress contraction. Layout and labels are the same as in (A).

(C) Comparison of the position of the persistence peak relative to the front part of the photoactivated region in controls or cells microinjected with C3 exotransferase or Y-27632 to suppress contraction for both active Cdc42 and active Rho. 0, peak at exact front; 1, peak at exact back. *$p < 0.05$; numbers indicate n.

(D) Quantification of total (i.e., of entire photoactivated regions) half-life of active Cdc42 or active Rho in controls or cells microinjected with C3 exotransferase or Y-27632 to suppress contraction. *$p < 0.05$; numbers indicate n. Error bars indicate SD.

turnover were accelerated enough to approach the dissipation rate for free probe, we would never know.

Contraction Helps Organize GTPase Activity

Although the GTPase signal treadmill can clearly operate in the absence of contraction, it just as clearly does so in an abnormal fashion, based on the slower and less organized closure of the contractile ring and the zones. To directly assess the contributions of contraction to the treadmill, the photoactivation approach was used in combination with contraction suppression via microinjection of C3 or Y-27632 for Cdc42 or Y-27632 for Rho. Photoactivation of the PA-GFP-GBD probes showed that, for both Cdc42 and Rho, suppression of contraction partially disorganized the treadmill (Figures 6A and 6B). Specifically, rather than the clear front-to-back persistence difference seen in controls, contraction suppression resulted in formation of discrete "islands" of active GTPases interspersed with regions of rapid loss of the active GTPases (Figures 6A and 6B, left panels), which was evident as the development of extra persistence peaks in kymographs (Figures 6A and 6B, right panels). The net result of this effect was a partial displacement of the persistence peak toward the trailing edge of the zones (Figure 6C).

Although both active Rho and Cdc42 displayed similar spatial patterns of disruption of the normal persistence pattern following contraction suppression, they differed with respect to the total half-life within the photoactivated region. That is, suppression of contraction slowed the loss of active Cdc42 but accelerated the loss of active Rho (Figure 6D). In sum, whereas contraction is dispensable for closure of the GTPase zones, it nonetheless contributes to the proper execution of the treadmill. The fact that the active GTPases are still preferentially recruited to the leading edge of the zones following contraction suppression (Figure 2) explains why the zones and rings can still close under conditions where treadmill organization is partially disrupted.

The GTPase Activity Gradients Are Entrained to F-Actin Turnover

If contraction is dispensable for closure of the GTPase zones, what serves as the basis of the GTPase treadmill? Because the ring of dynamic actin very closely follows the Cdc42 zone (Figure 2E; Figure S2; Movie S4), and because previous studies showed that suppression of F-actin turnover with jasplakinolide prevents closure of another kind of contractile array, the cytokinetic apparatus (Murthy and Wadsworth, 2005), we considered the possibility that F-actin turnover is required for the GTPase treadmill. To test this hypothesis, we assessed the effect of jasplakinolide treatment on the GTPase zones and on the contractile array. Strikingly, jasplakinolide resulted in the outward (i.e., away from the wound) spreading of the Rho and Cdc42 zones and a corresponding broadening of both the actin and the myosin-2 ring (Figures 7A and 7B; Figure S5). This resulted in abnormally broad contractile rings as well as abnormally broad zones (Figures 7A and 7B).

As a second test of this hypothesis, the photoactivation approach was applied to jasplakinolide-treated cells. Jasplakinolide treatment resulted in a sharp overall reduction of the half-life of active Rho within the broadened zone (Figure 7C) and eliminated the front-to-back difference in active Rho persistence (Figure 7D). Likewise, jasplakinolide also resulted in more

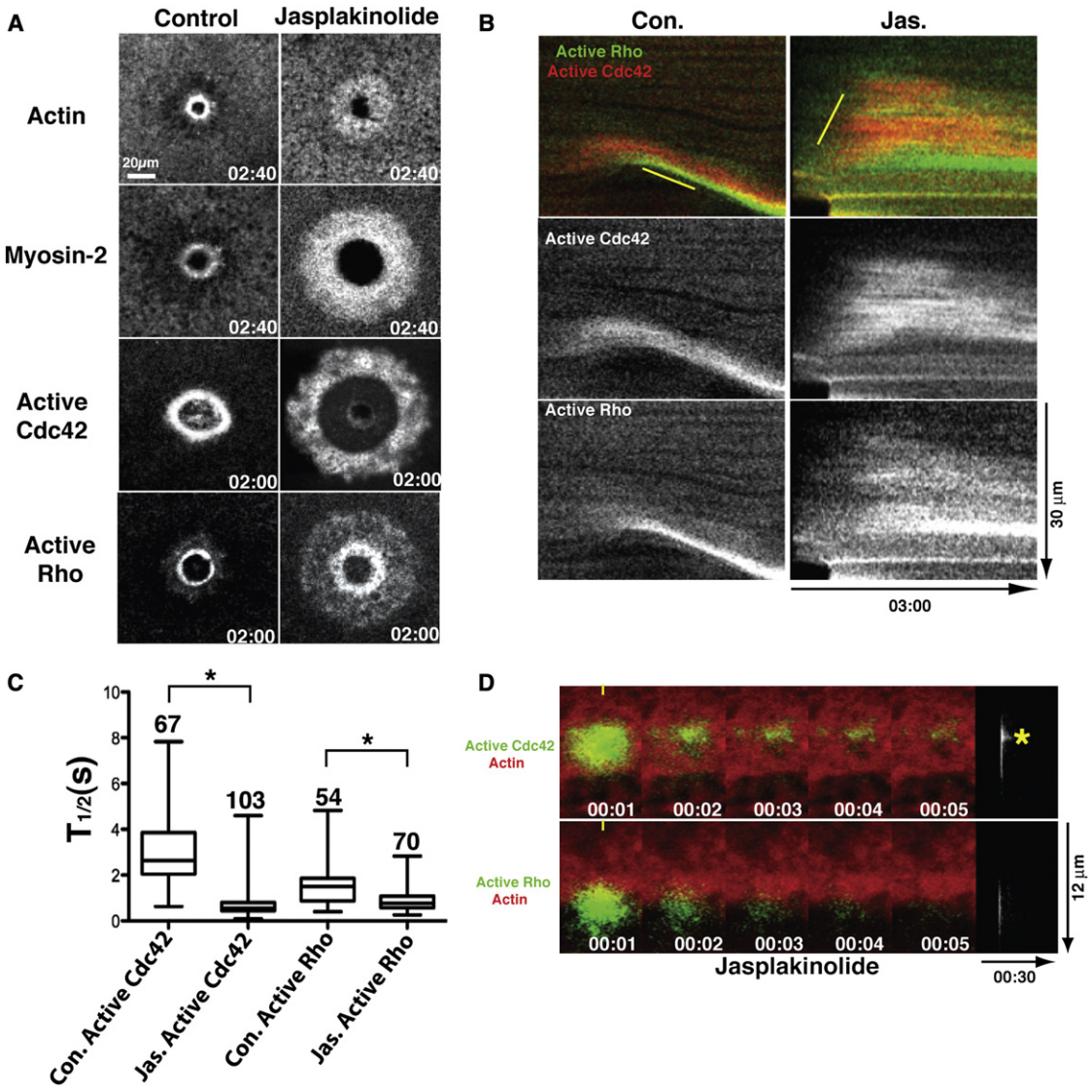

Figure 7. F-Actin Turnover Is Required for Proper Signal Treadmill Organization

(A) Matched time points showing distribution of actin, myosin-2, active Cdc42, or active Rho in control cells and cells treated with jasplakinolide to suppress F-actin turnover. Time is in min:s and refers to the time postwounding.

(B) Kymographs made using 1-pixel-wide line showing distribution of active Cdc42 and Rho in control (Con.) and jasplakinolide (Jas.)-treated cells. Top panels are double label, middle panels show active Cdc42 alone, and bottom panels show active Rho alone.

(C) Quantification of total (i.e., of entire photoactivated regions) half-life of active Cdc42 or active Rho in controls or cells treated with jasplakinolide to suppress F-actin turnover. *$p < 0.05$; numbers indicate n. Error bars indicate SD.

(D) Top-left panels show time points of active Cdc42 at wound edge assessed with PA-GFP-wGBD (green) and fluorescent actin (red) in presence of jasplakinolide. Top-right panel shows active Cdc42 alone as kymograph (prepared as in Figure 3) from same sample as on left. Asterisk indicates persistence peak. Bottom-left panels show time points of active Rho at wound edge assessed with PA-GFP-rGBD (green) and fluorescent actin (red) in presence of jasplakinolide. Bottom-right panel shows active Rho alone as kymograph (prepared as in Figure 3) from same sample as on left.

See also Figure S5.

rapid overall loss of active Cdc42 within the zone (Figure 7C). More remarkably, jasplakinolide treatment inverted the front-to-back polarity of the active Cdc42 persistence, such that the outer portion of the zone displayed more persistence than the inner zone (Figure 7D). Thus, F-actin turnover is necessary for the normal pattern of both GTPase activation and inactivation. Although it is likely that the change in myosin-2 distribution reflects the effects of jasplakinolide on Rho activity, it is also possible that some of the effects of jasplakinolide on the GTPases may, in turn, reflect feedback from the abnormally distributed myosin-2.

DISCUSSION

The first finding of this study—that a contractile array can close without contraction and without the movement of its

constituents—challenges the conventional view that contraction has the primary responsibility for steering a contractile array. Although it might be tempting to consider the wound-induced contractile arrays a special case, in fact they display the hallmarks of other contractile arrays including localized Rho activity, localized accumulation of active myosin-2, local cortical flow as well as springing open when broken (Mandato and Bement, 2001; Benink and Bement, 2005). It is therefore likely that the current findings will be applicable to other contractile arrays, a supposition consistent with work showing that inhibition of myosin-2-powered contraction does not necessarily prevent closure of cytokinetic arrays (Neujahr et al., 1997; Kanada et al., 2005; Reichl et al., 2008; Fang et al., 2010; Ma et al., 2012).

The second finding of this study—that Rho and Cdc42 within the zones move rapidly through the GTPase cycle—provides a direct demonstration of Rho family GTPase "flux." The GTPase flux model posits that activation and inactivation of the Rho family GTPases are closely coupled in space and time and is consistent with both theoretical and empirical studies (see Introduction). However, because fluorescently tagged Rho does not target properly to contractile arrays in vertebrates (e.g., Yonemura et al., 2004), visualization of Rho turnover has been hampered. The development and application of photoactivatable Rho and Cdc42 activity probes described here overcome this problem and indicate that Rho and Cdc42 are indeed subject to rapid local activation and inactivation within zones, with peak half-lives of ~8–12 s (Figure 5). Even more important is the form flux assumes. That is, modeling reveals that simply elevating the turnover rate of Rho family GTPases, combined with limitation of diffusion, is sufficient to generate the narrow GTPase zones observed during wound healing and cytokinesis (Bement et al., 2006). The signal treadmill revealed here shows that the process is more complex and suggests an obvious mechanism for steering closure of the contractile array: the array follows the treadmill. This is both intrinsically fascinating and suggestive of a broad analogy to F-actin and microtubules. That is, the point of nucleotide hydrolysis in each case is to bias the direction of assembly. For actin and tubulin, the bias is exerted at the level of the protein polymer; for the Rho family GTPases, the bias is exerted at the level of the subcellular contractile array controlled by the GTPases. Indeed, the analogy to polymers may be closer yet: the observation that farnesylated GFP flows inward as if it is anchored to the contractile array while the active GTPases remain largely stationary suggests that, at least while GTP bound, the GTPases might physically participate in an assembled superstructure. The obvious possibility for such a superstructure is the contractile array, suggesting the possibility that within this structure nodes—such as actin assembly or myosin recruitment sites—possibly remain more or less fixed while the network as a whole flows directionally.

A further level of sophistication emerges from comparison of the two GTPases. Rho behaves as if its activity zone is shaped by trailing edge inactivation, which is presumably due to localization of a Rho GAP in this region. Cdc42, in contrast, undergoes much more variable inactivation throughout its zone, as if GAP activity is elevated throughout its zone, and the zone is thus shaped predominantly by activation rather than inactivation.

The third finding of this study—that suppression of myosin-2-powered contraction disorganizes Rho and Cdc42 inactivation but does not prevent leading edge activation—explains the first finding. Contractile arrays can close without contraction (albeit more slowly and less precisely) because the GTPases are still preferentially activated at the leading edges of the zones despite the partial loss of the precise front-to-back persistence gradient. These results also reveal an unexpected role for myosin-2-powered contraction, namely, feedback control of GTPase inactivation. In essence, the idea is that contraction ensures its own orderly inactivation at the trailing edge of the Rho zone, presumably by organizing the relevant GAPs. The potential for myosin-2 to act as a dynamic F-actin organizer, or to provide tension, rather than serving solely as a shortener of F-actin arrays has been suggested from studies of cytokinesis (e.g., Murthy and Wadsworth, 2005; Reichl et al., 2008; Ma et al., 2012), and, as discussed below, a purely contractile function for myosin-2 in cytokinesis is not consistent with empirical observations.

The fourth finding of this study—that suppression of F-actin disassembly disrupts the normal pattern of both activation and inactivation of Rho and Cdc42—reveals that the treadmilling behavior of the GTPases is somehow entrained to F-actin turnover. Taken with the previous demonstration that inhibition of F-actin assembly does not prevent Rho and Cdc42 zone formation but does prevent their closure (Benink and Bement, 2005), and the observation that active Cdc42 leads actin (this study), these findings suggest that steering (closure) of the contractile apparatus is ultimately driven by feedback between GTPase activity and differential actin assembly and disassembly, rather than contraction per se. That is, preferential activation of Rho and Cdc42 at the leading edges of the zones results in preferential actin assembly, which in turn promotes further GTPase activation. Suppression of assembly stalls the zones, whereas suppression of disassembly leaves only the free outer edge of the Cdc42 zone available for new assembly, thus resulting in a transient reversal of the normal pattern of zone displacement. If this general model is correct, it argues for the existence of GEFs and GAPs that are directly or indirectly regulated by assembling and disassembling F-actin and/or F-actin in different nucleotide states (e.g., bound to ATP versus ADP-Pi, or ADP). Furthermore, because the Rho and Cdc42 zones are separated in space and display differences in their flux behavior, it also follows that each zone will employ different subsets of players to regulate actin assembly.

This model can explain puzzling features of other processes based on contractile arrays such as cytokinesis. As observed some time ago, simultaneously lengthening and ingression of contractile arrays is difficult to explain in a standard purse string model (Schroeder, 1990). It is, however, consistent with a mechanism wherein differential assembly/disassembly of F-actin directs ingression. Furthermore, several studies show that cytokinesis can occur in the absence of Rho or myosin-2 motor activity (see above), although the process is slower and less organized than the normal situation, similar to the results observed here following contraction suppression. We therefore suggest that the closure of the cytokinetic apparatus under conditions of suppressed contractility, as observed here for single-cell wound repair, is driven by differential F-actin turnover entrained to a Rho treadmill. Likewise, we propose that the broadening and stalling of the cytokinetic apparatus observed following jasplakinolide treatment (Murthy and Wadsworth,

2005) reflect broadening and stalling of local Rho activity, as observed in this study.

Finally, the inward, wave-like movement of the GTPase zones and the contractile array observed following suppression of contraction and the sensitivity to disruption of F-actin turnover is reminiscent of the behavior of locomoting cells in that the primary means of ingression appears to be based on actin turnover. The basic conservation of the players and regulatory mechanisms for cytokinesis and cell locomotion has been pointed out previously (Rodriguez et al., 2003; Janetopoulos and Devreotes, 2006); the results presented here are consistent with this idea and indicate that contractile arrays are generally controlled by the same mechanisms that drive cell locomotion, with the major differences resulting from spatial organization of the regulatory players, rather than fundamental differences in the players themselves.

EXPERIMENTAL PROCEDURES

Oocyte Collection and Drug Treatments

Oocytes were harvested from adult *Xenopus laevis* frogs, manually defolliculated after collagenase treatment, and stored in 1× Barth's solution (88 mM NaCl, 1 mM KCl, 2.4 mM NaHCO3, 0.82 mM MgS04, 0.33 mMCaN03, 0.41 CaCl2, 10 mM HEPES [pH 7.4]). *Xenopus laevis* were maintained and utilized under the oversight of the University of Wisconsin-Madison Animal Care and Use Committee. Microinjections were performed with a Harvard Apparatus p-100 microinjector. A total of 2 ng of C3 exotransferase (cytoskeleton), 68 ng of Y-27632 (Calbiochem), or 5 ng Blebbistatin (Tocris) was injected 15–20 min prior to wounding. Blebbistatin-treated cells were also incubated in fresh 100 μm Blebbistatin/Barth's solution before and after microinjection. Blebbistatin use was restricted to experiments with red (e.g., RFP) probes because the blue light required for imaging green (e.g., EGFP) probes inactivates blebbistatin (Kolega, 2004). A total of 40 nl of 20 mM GTPγS was injected 20 min before imaging.

Fluorescent Reporters and Proteins

Photoactivatable reporters for active Rho and Cdc42 were generated by linking PA-GFP (Patterson and Lippincott-Schwartz, 2002) to rGBD and wGBD, respectively. PA-fGFP was generated by attaching the ras farnesylation signal to PA-GFP. GFP-rGBD and mRFP-wGBD (Benink and Bement, 2005), GFP-Utr-CH (Burkel et al., 2007) and the photoactivatable probes were transcribed in vitro using the SP6 mMessage machine (Ambion). PA-GFP-rGBD and PA-GFP-wGBD also underwent an additional poly A-tailing reaction (Ambion) that was verified by a denaturing agarose gel. PA-GFP mRNAs were allowed to express for 48–72 hr at 16°C and all other mRNAs expressed for 24 hr at 16°C. To monitor actomyosin ring localization and zone movement, 40 nl of 0.25 μg/μl Alexa 568-actin (Invitrogen) was injected the same day of mRNA injections. To monitor myosin distribution, 40 nl of 1 mg/ml TMR-myosin-2 was microinjected 4–24 hr prior to imaging.

Wounding, Photoactivation, Image Acquisition, and Analysis

Experiments highlighting contractile array and GTPase zone movement (six optical planes; 1 fps) were conducted with a Zeiss Axiovert confocal fitted with a nitrogen-pumped dye laser (Laser Science) for wounding. Photoactivation experiments (one optical plane, 1fps) were conducted using an Olympus FluoView-1000 with the auxiliary sim scanner. Wounding was accomplished by using the 405 nm line at 80% of the maximum for 150 ms, except for experiments with the PA-fGFP and those involving jasplakinolide, in which cases cells were wounded with a 440 nm nitrogen pump dye laser to reduce background noise and then transferred to the Olympus FluoView for imaging. To photoactivate the various reporters, the 405 nm line was used at 5% of maximum for 150 ms. 4D movies were generated using Volocity 5.0. Kymographs, brightest-point projections, and measurements of fluorescence intensities and distances were made using ImageJ. GraphPad Prism was used for statistical analysis and determination of half-times. One or two decay exponentials were used to derive half-times, where appropriate. One-way ANOVA with a Tukey post hoc analysis was used for comparisons involving multiple groups. The measure function was used to measure distance and angle of the contractile ring or flowing particles, from which velocities were derived. The multiple velocities were averaged per wound and then compiled with other wounds for statistical analysis. The rearward shift of fluorescence peaks was calculated by measuring the distance to the peak of longest fluorescence persistence and dividing it by the total distance of the PA spot. Front:back ratios and fluorescence persistence measurements were made at the first and third quartile of the photoactivated spot. ImageJ was then used to measure the distance and then derive a fluorescence persistence. Contractile ring organization was quantified by first thresholding with ImageJ, and then tracing and measuring the perimeter and wound area. This measured perimeter to measured wound area was then divided by the ideal (circular) perimeter over the wound area of the same size.

SUPPLEMENTAL INFORMATION

Supplemental Information includes five figures and five movies and can be found with this article online at http://dx.doi.org/10.1016/j.devcel.2012.05.025.

ACKNOWLEDGMENTS

The authors are grateful to their laboratory mates, who have long been ready sources of advice, encouragement, and entertainment. This work was supported by NIH GM52932 to W.M.B. and MCB-0917887 to G.v.D.

Received: March 7, 2012
Revised: May 12, 2012
Accepted: May 29, 2012
Published online: July 19, 2012

REFERENCES

Abreu-Blanco, M.T., Verboon, J.M., and Parkhurst, S.M. (2011). Cell wound repair in *Drosophila* occurs through three distinct phases of membrane and cytoskeletal remodeling. J. Cell Biol. *193*, 455–464.

Bement, W.M., Miller, A.L., and von Dassow, G. (2006). Rho GTPase activity zones and transient contractile arrays. Bioessays *28*, 983–993.

Benink, H.A., and Bement, W.M. (2005). Concentric zones of active RhoA and Cdc42 around single cell wounds. J. Cell Biol. *168*, 429–439.

Burkel, B.M., von Dassow, G., and Bement, W.M. (2007). Versatile fluorescent probes for actin filaments based on the actin-binding domain of utrophin. Cell Motil. Cytoskeleton *64*, 822–832.

Chuang, T.H., Xu, X., Kaartinen, V., Heisterkamp, N., Groffen, J., and Bokoch, G.M. (1995). Abr and Bcr are multifunctional regulators of the Rho GTP-binding protein family. Proc. Natl. Acad. Sci. USA *92*, 10282–10286.

Clark, A.G., Miller, A.L., Vaughan, E., Yu, H.Y., Penkert, R., and Bement, W.M. (2009). Integration of single and multicellular wound responses. Curr. Biol. *19*, 1389–1395.

Fang, X., Luo, J., Nishihama, R., Wloka, C., Dravis, C., Travaglia, M., Iwase, M., Vallen, E.A., and Bi, E. (2010). Biphasic targeting and cleavage furrow ingression directed by the tail of a myosin II. J. Cell Biol. *191*, 1333–1350.

Jaffe, A.B., and Hall, A. (2005). Rho GTPases: biochemistry and biology. Annu. Rev. Cell Dev. Biol. *21*, 247–269.

Janetopoulos, C., and Devreotes, P. (2006). Phosphoinositide signaling plays a key role in cytokinesis. J. Cell Biol. *174*, 485–490.

Kanada, M., Nagasaki, A., and Uyeda, T.Q. (2005). Adhesion-dependent and contractile ring-independent equatorial furrowing during cytokinesis in mammalian cells. Mol. Biol. Cell *16*, 3865–3872.

Kolega, J. (2004). Phototoxicity and photoinactivation of blebbistatin in UV and visible light. Biochem. Biophys. Res. Commun. *320*, 1020–1025.

Ma, X., Kovács, M., Conti, M.A., Wang, A., Zhang, Y., Sellers, J.R., and Adelstein, R.S. (2012). Nonmuscle myosin II exerts tension but does not

translocate actin in vertebrate cytokinesis. Proc. Natl. Acad. Sci. USA *109*, 4509–4514.

Mandato, C.A., and Bement, W.M. (2001). Contraction and polymerization cooperate to assemble and close actomyosin rings around *Xenopus* oocyte wounds. J. Cell Biol. *154*, 785–797.

Martin, A.C., Kaschube, M., and Wieschaus, E.F. (2009). Pulsed contractions of an actin-myosin network drive apical constriction. Nature *457*, 495–499.

McNeil, P.L., and Steinhardt, R.A. (2003). Plasma membrane disruption: repair, prevention, adaptation. Annu. Rev. Cell Dev. Biol. *19*, 697–731.

Miller, A.L., and Bement, W.M. (2009). Regulation of cytokinesis by Rho GTPase flux. Nat. Cell Biol. *11*, 71–77.

Minoshima, Y., Kawashima, T., Hirose, K., Tonozuka, Y., Kawajiri, A., Bao, Y.C., Deng, X., Tatsuka, M., Narumiya, S., May, W.S., Jr., et al. (2003). Phosphorylation by aurora B converts MgcRacGAP to a RhoGAP during cytokinesis. Dev. Cell *4*, 549–560.

Munro, E., Nance, J., and Priess, J.R. (2004). Cortical flows powered by asymmetrical contraction transport PAR proteins to establish and maintain anterior-posterior polarity in the early *C. elegans* embryo. Dev. Cell *7*, 413–424.

Murthy, K., and Wadsworth, P. (2005). Myosin-II-dependent localization and dynamics of F-actin during cytokinesis. Curr. Biol. *15*, 724–731.

Neujahr, R., Heizer, C., and Gerisch, G. (1997). Myosin II-independent processes in mitotic cells of Dictyostelium discoideum: redistribution of the nuclei, re-arrangement of the actin system and formation of the cleavage furrow. J. Cell Sci. *110*, 123–137.

Patterson, G.H., and Lippincott-Schwartz, J. (2002). A photoactivatable GFP for selective photolabeling of proteins and cells. Science *297*, 1873–1877.

Rauzi, M., Lenne, P.F., and Lecuit, T. (2010). Planar polarized actomyosin contractile flows control epithelial junction remodelling. Nature *468*, 1110–1114.

Reichl, E.M., Ren, Y., Morphew, M.K., Delannoy, M., Effler, J.C., Girard, K.D., Divi, S., Iglesias, P.A., Kuo, S.C., and Robinson, D.N. (2008). Interactions between myosin and actin crosslinkers control cytokinesis contractility dynamics and mechanics. Curr. Biol. *18*, 471–480.

Rodriguez, O.C., Schaefer, A.W., Mandato, C.A., Forscher, P., Bement, W.M., and Waterman-Storer, C.M. (2003). Conserved microtubule-actin interactions in cell movement and morphogenesis. Nat. Cell Biol. *5*, 599–609.

Schroeder, T.E. (1973). Actin in dividing cells: contractile ring filaments bind heavy meromyosin. Proc. Natl. Acad. Sci. USA *70*, 1688–1692.

Schroeder, T.E. (1990). The contractile ring in furrowing and dividing cells. Ann. N. Y. Acad. Sci. *582*, 78–87.

Sokac, A.M., Co, C., Taunton, J., and Bement, W. (2003). Cdc42-dependent actin polymerization during compensatory endocytosis in *Xenopus* eggs. Nat. Cell Biol. *5*, 727–732.

Sonnemann, K.J., and Bement, W.M. (2011). Wound repair: toward understanding and integration of single-cell and multicellular wound responses. Annu. Rev. Cell Dev. Biol. *27*, 237–263.

Straight, A.F., Cheung, A., Limouze, J., Chen, I., Westwood, N.J., Sellers, J.R., and Mitchison, T.J. (2003). Dissecting temporal and spatial control of cytokinesis with a myosin II Inhibitor. Science *299*, 1743–1747.

Uehata, M., Ishizaki, T., Satoh, H., Ono, T., Kawahara, T., Morishita, T., Tamakawa, H., Yamagami, K., Inui, J., Maekawa, M., and Narumiya, S. (1997). Calcium sensitization of smooth muscle mediated by a Rho-associated protein kinase in hypertension. Nature *389*, 990–994.

Vaughan, E.M., Miller, A.L., Yu, H.Y., and Bement, W.M. (2011). Control of local Rho GTPase crosstalk by Abr. Curr. Biol. *21*, 270–277.

Yonemura, S., Hirao-Minakuchi, K., and Nishimura, Y. (2004). Rho localization in cells and tissues. Exp. Cell Res. *295*, 300–314.

Yoshida, S., Bartolini, S., and Pellman, D. (2009). Mechanisms for concentrating Rho1 during cytokinesis. Genes Dev. *23*, 810–823.